Structure and Function of Oligomeric Dehydrogenases. Electron Microscopic Studies of Beef Liver Glutamate Dehydrogenase Quaternary Structure*

A. Max Fiskin,† E. F. J. van Bruggen, and Harvey F. Fisher

ABSTRACT: Alternative models of the quaternary structure of bovine glutamate dehydrogenase (GDH) have been deduced from electron microscopic projections of the enzyme stained negatively and positively with uranyl salts. The formate salt gives optimum resolution of substructure with uranyl negative stains at 1000-Å under-focus and three stages of photographic contrast enhancement. Negatively stained GDH gives three catagories of projections; two with apparent threefold axes. The intensity distribution in all projections indicate the oligomer is composed of at least ten regions not penetrated by stain.

A survey of possible models, with image simulation by either light shadowgraphs or a refined X-ray shadowgraphic analog, indicates that the oligomer is composed of twelve masses (fold-ons), arrayed at the vertices of either an icosahedron or of the closely related cuboctahedron. The images can be simulated with either tetrahedral models composed of four trimeric subunits or octahedral models composed of six dimeric subunits. Projections of GDH positively stained with a variety of heavy metal salts appear hexagonal, while particles partially disrupted in staining give projections corresponding to the dominant projection in negative stain. X-Ray shadowgraph analogs of positive staining of models in either icosahedral or cuboctahedral arrays give projections equivalent to the micrographs. Dissociation of the oligomer in 3 mM sodium dodecyl sulfate preserves a compact subunit tertiary structure, and suboligomers of the enzyme composed of three or four masses of roughly equivalent size are observed microscopically. The dimensions—35 ± 5 Å (contact to contact) for the fold-ons and 95 ± 5 Å for the oligomer—and symmetry properties of the proposed models are consistent with the physical-chemical character of GDH and its aggregates.

The dehydrogenases, enzymes with molecular weights lying in the range 20,000 to 500,000, provide a particularly well-characterized system for studying the relationships between structure and function in oligomeric enzymes. Detailed studies of molecular weights, subunit compositions, and optical properties, as well as of enzymatic properties, have been performed on most known dehydrogenases. As a result of the theoretical controversy (Koshland *et al.*, 1966; Kirtley and Koshland, 1967; Monod *et al.*, 1964; Haber and Koshland, 1967) over relating quaternary symmetry to the function of enzymes, attention is currently focused on possible correlations between allosteric properties of the dehydrogenases and the relatively uncharacterized quaternary structures of these enzymes. Studies of a variety of protein structures (*e.g.*, Fernandez-Moran *et al.*, 1966; Valentine *et al.*, 1968; Haydon, 1969) have demonstrated the potential and pitfalls of deducing quaternary structure from high-resolution electron microscopic visualization of proteins stained with heavy metal.

Whitehead (1965) has proposed an underlying order relating the quaternary structures of the various pyridine nucleotide dehydrogenases. In order to explain the structure of dehydrogenases comprised of subunits known to be several times larger than the morphopoietic unit he postulates, Whitehead proposes that these subunits consist of several covalently bonded component masses of about 20,000 molecular weight. A spherical protein particle with this molecular weight would have a diameter of about 35 Å, *i.e.*, a dimension greater than the resolutions obtained in electron microscopic studies of negatively stained protein particles. This suggests that the "fold-on"[1] concept of dehydrogenase quaternary structure may be tested electron microscopically; and, indeed, Horne and Greville (1963) have presented micrographs of GDH[2] negatively stained with phosphotungstic acid which could be interpreted as corroborating a fold-on structure for this enzyme.

* Research Laboratories, Veterans Administration Hospital, Kansas City, Missouri; Laboratory for Structural Chemistry, University of Groningen, The Netherlands; and Department of Biochemistry and Microbiology, University of Kansas School of Medicine, Kansas City, Kansas. *Received August 31, 1970.* This research was supported in part by Grant GB 7862 from the National Science Foundation and Grant GM 15188 from the National Institutes of Health and supported in part by Postdoctoral Fellowship GM-15,403 from the National Institute of General Medical Sciences, U. S. Public Health Service. Preliminary reports on portions of this work were presented before the American Chemical Society, Atlantic City, 1968, and the Isozyme Conference, Galveston, Dec 1968.

† Present address: Biophysics Laboratory, Veterans Administration Hospital, Kansas City, Mo. 64128; to whom to address correspondence.

[1] Several nomenclatures have been proposed for the levels of GDH structure (Frieden, 1964). The system used here follows Fisher (1969) and the terminology of Klotz *et al.* (1970): δ, for the individual polypeptide chain, or subunit, observed in urea, etc; β, for the oligomer, composed of four to seven δ units, observed in dilute GDH solutions; α, for aggregates of β units observed at concentrations above 0.1 mg/ml; and γ, for a form of intermediate molecular weight, composed of two or three δ units, observed when the β unit is dissociated by DPNH. The text uses α and β as morphological designations, but, as described in the discussion of dissociated β units, it is less clear which dissociated species are observed microscopically, so they are generically named "suboligomers." Physical chemical studies have suggested that the tertiary structure of some proteins is in the form of several polypeptide masses joined covalently, *e.g.*, subtilism. J. Kraut (personal communication, University of California at San Diego) suggests the term "fold-on" for any one of the covalently linked polypeptide masses of such peptide chains.

[2] Abbreviations used are: GDH, glutamate dehydrogenase, or L-glutamate:NAD(P) oxidoreductase (deaminating) (EC 1.4.1.3); SDS, sodium dodecyl sulfate.

The structural complexity of GDH has been studied extensively since the reversible association of the β^1 units was described by Olsen and Anfinsen (1952). The β unit can be dissociated into δ^1 units by SDS (Jirgensons, 1961), urea, and guanidine hydrochloride (Wolff, 1962; Frieden, 1962; F. J. Reitel, personal communication), and acid or alkali (Fisher *et al.*, 1962; Fisher and Cross, 1962). Molecular weight studies of the GDH oligomer (280,000, Sund and Burchard, 1968; 313,000, Eisenberg and Tomkins, 1968) and the polypeptide chains (53,000, Eisenberg and Tomkins, 1968; 56,000, Smith *et al.*, 1970), and studies of the polypeptide sequence (Smith *et al.*, 1970) and end groups (Jirgensons, 1961; Apella and Tomkins, 1966) of GDH, suggest that the oligomer has five or six identical subunits.

This paper reports on the first of a series of high-resolution electron microscopic studies of quaternary structure in oligomeric dehydrogenases, directed specifically to determining if the structures are based on a fold-on morphopoietic unit, and to relating structure and function in these enzymes. Electron microscopic projections of the functional oligomer (β) of GDH, positively and negatively stained with uranyl salts, and of the intact subunits (δ) positively stained with uranyl salts, are compared to simulated projections of model systems irradiated with visible or X-ray radiation. The X-ray shadowgraph procedure described permits simulation of many of the anticipated disruptive effects of heavy metal on protein particles, and comparison of the X-ray projections of models with the electron images provides conclusive evidence that there are more than one component masses (morphological units) per subunit of GDH. An extensive survey with X-ray simulation of possible models is described, alternative models for the quaternary structure consistent with the electron images of GDH are presented, and the symmetry properties of the models are discussed. Studies of the dimensions of platinum shadows of GDH aggregates will be presented elsewhere.

Materials and Methods

Bovine liver glutamate dehydrogenase (GDH) was obtained from Boehringer und Sohne, both as the ammonium sulfate suspension and as the glycerol solution. Uranyl acetate, ammonium acetate, mercuric and potassium iodide, thallous bicarbonate, formic acid, and oxalic acid were from Fisher Scientific. All solutions were prepared in water doubly distilled in a Hereaus all quartz apparatus. Uranyl oxalate was prepared as described by Mellema *et al.* (1967). Uranyl formate was prepared from the acetate by precipitating the hydroxide by titration with NH_4OH, and back-titration of the washed precipitate with formic acid to pH 4.0. All solutions were filtered through 0.22 μ Millipore prior to use.

Enzyme Solutions. GDH solutions were prepared from the glycerol solution by exhaustive dialysis against a solution designed for optimum stability of GDH activity (solution A: 3×10^{-4} M ADP, 5×10^{-3} M $(NH_4)_2SO_4$, and 5×10^{-3} M glutamate, adjusted to pH 7.6, with NH_4OH). Solutions were prepared from the ammonium sulfate suspension either by dissolving the centrifuged pellet in solution A, or by dialyzing directly against solution A without ammonium sulfate, to give a final ammonium sulfate concentration of 5×10^{-3} M. The GDH solutions were prepared as 10-mg/ml stock solutions, which were diluted to the experimental concentrations with solution A immediately prior to grid preparation. The activity of the stock solutions was checked routinely by dialyzing aliquots against phosphate buffer (pH 7.6) and measuring initial velocities of conversion of DPNH into DPN spectrophotometrically at 340 mμ (6×10^{-5} M DPNH (Sigma), 0.1 M NH_4Cl, 10^{-4} M EDTA, and 0.25 M α-ketoglutaric acid). All enzyme solutions were filtered through 0.22 μ Millipore filters and stored at 8°.

Solutions of Relatively Undenatured GDH Suboligomers. A stock solution of 10 mg/ml of GDH in solution A was diluted with SDS in 0.1 M ammonium acetate (pH 7.6) to a final concentration of 2 mg of protein/ml of 3.0 mM SDS. The mixture was allowed to set at room temperature for 1 hr and diluted 1:200 with 0.04 M β-mercaptoethanol in 0.01 M ammonium acetate (pH 7.6; final concentrations 0.01 mg of protein/ml of 0.015 mM SDS and 0.04 M β-mercaptoethanol).

Specimen Support Films. Ultrathin carbon films were prepared by evaporation under vacuum onto freshly cleaved mica, either directly (in the Varian Vac-Ion system, 10^{-8} torr) or indirectly by reflection from glass (in a Hitachi HUS-3). The films were floated off the mica strips onto either quartz distilled, Millipore-filtered water, or directly onto protein solutions, as described below.

Grid Preparation. Carbon substrates were picked up on 400-mesh copper grids cleaned by sonication (acetone–water–H_2SO_4 (0.1 M)–water–acetone). For studies of protein particles dried on the film prior to treatment with heavy metal solutions, the carbon surfaces of the grids were streaked over the protein solution as described previously (Fiskin and Beer, 1968) in an attempt to (a) minimize the volume of protein solution adhering to the surface and (b) establish a preferred orientation of linear aggregates on the grid. In our hands the best structural information was obtained by depositing negative stain layers (either 0.5 or 1% uranyl acetate, formate, or oxalate) onto substrates bearing dried protein. This was accomplished by both the drop method and spraying the uranyl salt solution in the cold. Less satisfactory results were obtained by spraying enzyme–uranyl salt mixtures or by the method of Valentine *et al.* (1968). Protein dried on substrate was positively stained by floating on uranyl solutions, then streaking the grid over the surface of the staining dish as described above to remove excess stain solution, then drying them with substrate side down on filter paper.

Electron Microscopy. The studies of the suboligomers of GDH were performed on a Hitachi HU 11B electron microscope equipped with a liquid nitrogen cold trap, operated with 75-kV accelerating voltage and 40-μ objective apertures. The balance of the microscopy was performed with a Philips EM 200 equipped with a liquid nitrogen cold trap, operated with 80-kV accelerating voltage and 40-μ objective apertures. All grids were sprayed with latex spheres to facilitate correction of objective astigmatism to less than 500 Å. For high-resolution studies, through-focal series weret aken of each specimen area, and magnification was calibrated daily with a standard grating replica (Ladd). Photographic contrast enhancement was performed in three to five stages, as described previously (Fiskin and Beer, 1968). Image dimensions of the particles were determined with a Zeiss particle size analyzer, Model TGZ3.

Analogs for Simulating Electron Images. Figure 6 describes the light shadowgraph method used. The individual balls which comprise the models represent postulated protein cores into which heavy metal cannot penetrate, while the spaces between those balls represent postulated loosely organized protein or void spaces through which heavy metal can move.

The X-ray shadowgraph procedure employs models built from X-ray transparent polystyrene spheres, which provide the analog for fold-ons. The models are sewn together with rigid intrasubunit fold-on contacts, but with elastic intersub-

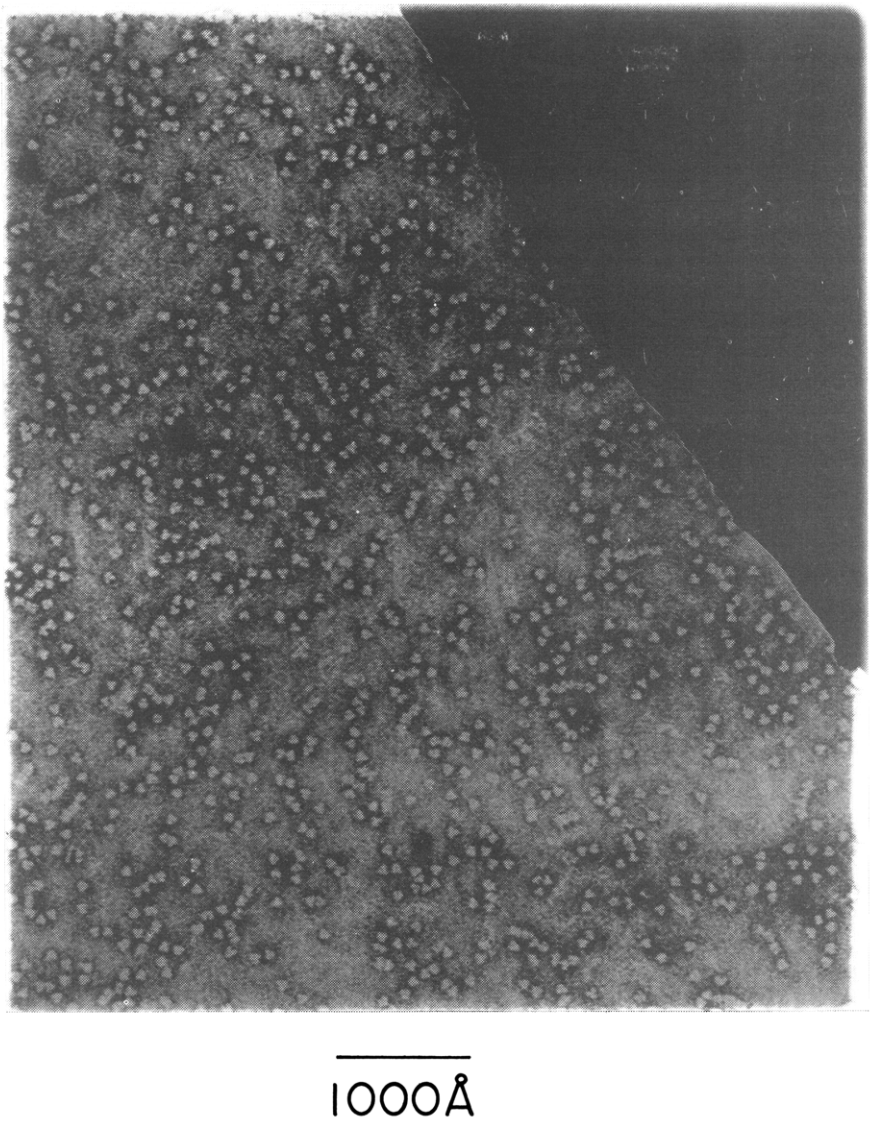

FIGURE 1: GDH stained negatively with 1% uranyl acetate. Protein deposited from solution of 0.05 mg of GDH/ml of solution A. 166,500×.

unit contacts. The models are easily distorted or disrupted through the contacts between subunits, permitting a variety of possible drying and stain disruption effects to be tested. The negative stain layer is simulated by layers of various sizes of X-ray opaque marbles. The models were either held to the bottom of an X-ray transparent container and submerged to desired levels with marbles, or immersed in the marble layer. The orientation of the model relative to the direction of radiation was determined with the container placed on an X-ray film cassette, and the assembly was irradiated with a Continental Model EH-S portable X-ray unit. The exposure time and level of radiation was calibrated to give the single marble contrast appropriate to the size its dimensions represent in the simulation (Haine, 1961). The effects of penetration of heavy metal into the particle are simply simulated by disrupting the elastic intersubunit bonds by inserting marbles.

Results and Discussion

Enhancement of Information from the Micrographs. It has been shown, both in theory and in practice, that phase contributions to intensity permit contrast enhancement by defocusing electron images (Heidenreich, 1964). Images of GDH in uranyl acetate, formate, and oxalate negative stains were studied as a function of degree of under-focus in an effort to define conditions for balancing (a) maximum particle contrast relative to contrast in the stain layer and (b) minimum distortion or blurring of detail relative to gaussian focus.[3] Moderately thin carbon films, which are extensively characterized in the literature in terms of phase contrast as a function of defocus, were used throughout. Previous studies (Highton and Beer, 1968) compared the rate of increase in contrast arising from point deposits of heavy metal on polynucleotides, to the rate of increase in contrast arising from carbon supporting films, as a function of defocus. An optimum signal-to-noise ratio was demonstrated at 500–700-Å under-focus. When applied in conjunction with multistage photographic contrast enhancement, these conditions permitted determination of the internucleotide spacing in linearly extended polynucleotides (Fiskin and Beer, 1968). However, the spatial amplitude of phase-contrast "noise" from layers of heavy metal deposited on carbon films increases more rapidly with defocus than that from the carbon films alone, and there is no *a priori* basis for

[3] Preparations with sprayed-enzyme-stain solutions were unsatisfactory due to precipitation of enzyme, even in dilute (0.1 M) uranyl salts; the micrographs used in the analysis were of specimens prepared by the drop method.

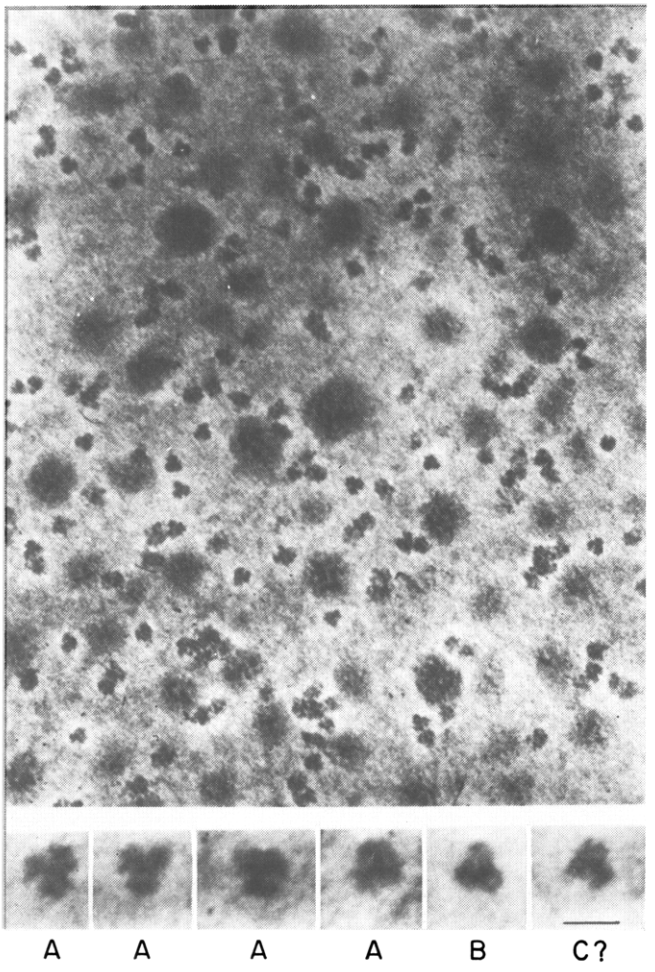

FIGURE 2: GDH stained negatively with 1% uranyl formate (in-focus). Protein deposited from solutions 0.05 mg of GDH/ml of solution A. A, B, and C refer to projection categories defined in the text. Micrograph at focus (±100 Å). Magnifications 271,000× and 740,000× (inserts). Bar = 100 Å.

assuming optimum focus will occur in the same range as for positive staining.

Figure 1, a moderate resolution micrograph of GDH projections in uranyl acetate, is characterized by (a) predominance of propeller shaped monomer projections closely resembling those observed in phosphotungstate (Horne and Greville, 1963); (b) apparently exclusive end-to-end aggregation (to be described elsewhere); and (c) a high-stain layer background noise level at moderate (1500 Å) under-focus. As reported by others, at far under-focus (2–3 μ) the contrast of (protein) regions excluding heavy metal becomes high relative to the stain layer, but detail in the image is blurred and contours distorted. Because of the high-noise figure the optimum conditions (as defined above) for contrast enhancement with the acetate salt occur at less than 500-Å under-focus, where definition of contrast detail within particles was mediocre. Uranyl oxalate stain layers gave comparatively low-background noise, but GDH particle projections appeared circular or hexagonal with poorly defined substructure, suggesting the oxalate salt penetrates into the particles less readily than the acetate or formate salts.

Figure 2 is a micrograph at focus of GDH in uranyl formate. The projections resemble those in uranyl acetate, *i.e.*, a predominance of propeller-shaped projections in which each blade of the propeller is composed of two to four maxima.

FIGURE 3: GDH stained negatively with 1% uranyl formate, focal effects. Protein deposited from solutions of 0.05 mg of GDH/ml of solution A. (a) 2000 ± 100 Å under-focus; (b) 1000 ± 100 Å under-focus; and (c) focus ± 100 Å. a′,b′, and c′, optical density contours of a typical particle projection (arrow) in the respective members of the series. The projection was scanned linearly at 1-mm intervals on a Joyce-Lobel automatic recording densitometer, spot size 1 mm², and relative optical densities plotted on a 1-mm grid to permit contours to be drawn. After three stages of photographic contrast enhancement, magnification 2,440,000×. Bar = 100 Å.

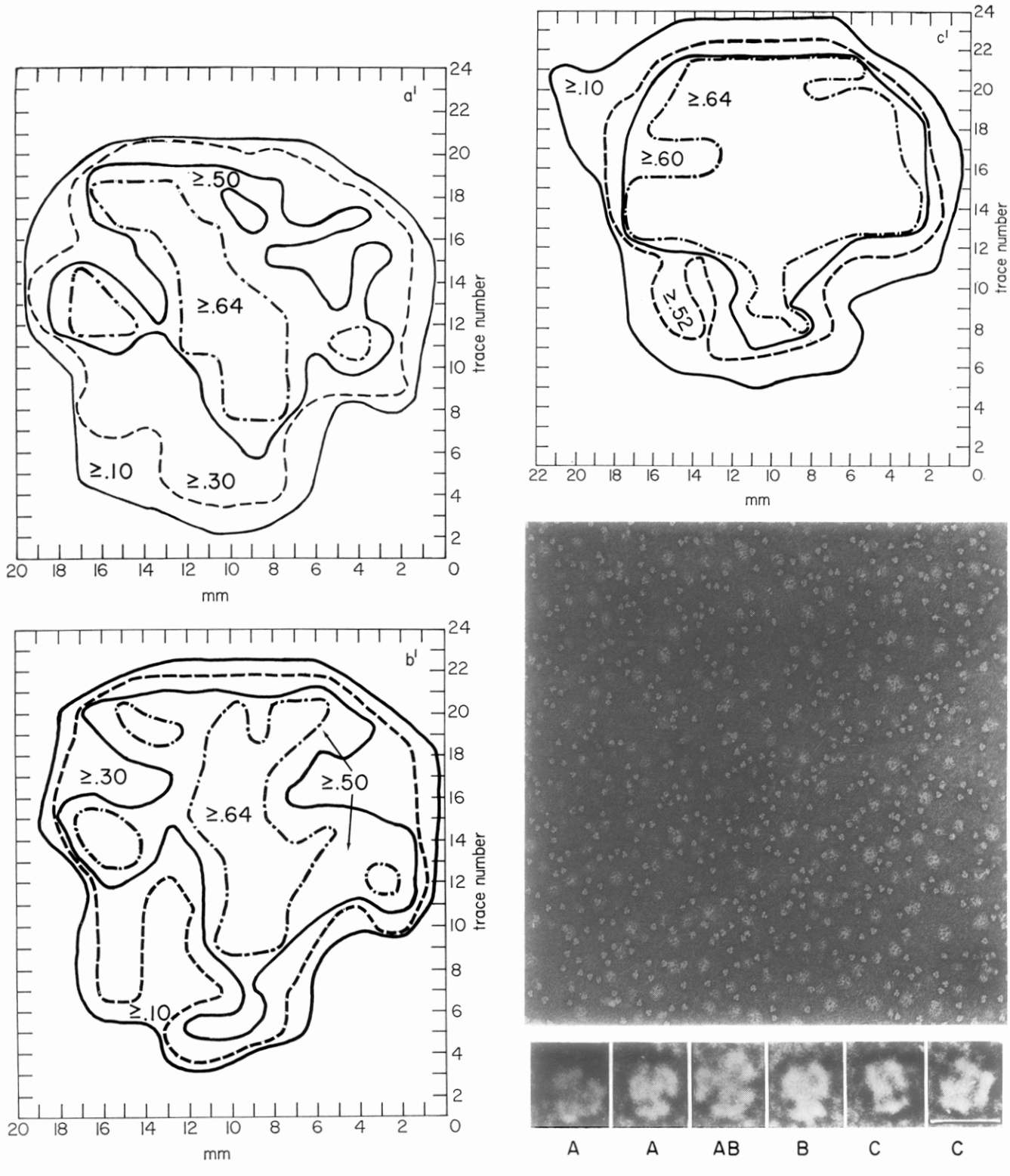

FIGURE 4: GDH stained negatively with 1% uranyl formate. A, B, AB, and C refer to projection categories defined in the text. Standard photographic enlargement, to magnifications of 98,520× and 1,259,000× (inserts). Bar = 100 A.

Most particle projections are surrounded by a halo of low intensity, but the intensity and width of the halo varies from particle to particle, suggesting that it arises from a real difference in mass density of the layer around the particle, rather than from an electron-optical effect.

Figure 3a–c was selected from a through-focal series of GDH in uranyl formate to demonstrate the variation in contrast of particle projections in this stain, with focus, after photographic contrast enhancement. Figure 3a′–c′ map the optical density contours within a typical monomer projection in each of the respective micrographs. At ~2000-Å under-focus it is evident that although contrast is very high, the contours and dimensions of the intensity maxima within the particle projections differ appreciably from those in the near-focus

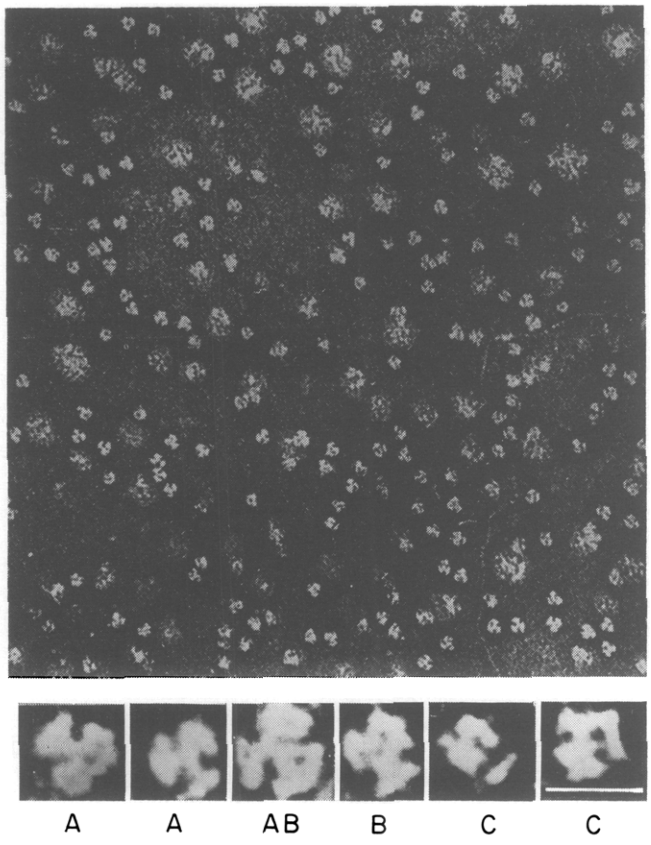

FIGURE 5: GDH stained negatively with uranyl formate. A, B, AB, and C refer to projection categories defined in the text. After three stages of photographic contrast enhancement, magnifications 238,570× and 1,271,000× (inserts). Bar = 100 Å.

image, and the intensity and dimensions of the phase noise figure from the stain layer are comparable to those in the particle projections. The optimum under-focus for contrast enhancement for the formate salt is represented by the ~1000-Å under-focus micrograph, where the definition and intensity of the maxima in the particle projections is much higher than in the near-focus image, and distortion of the dimensions of the maxima due to smoothing of contours is negligible. For this focal range, the enhancement procedure gives maxima intensities within the projections which are significantly greater than those of the noise figure. Figures 4 and 5 show GDH in uranyl formate, at ~1000-Å under-focus, with and without photographic contrast enhancement, respectively. Point by point comparison of the two figures confirms that the enhancement procedure preserves the precise location of the intensity maxima, while sacrificing little contour detail.

Projections in Negative Stain. Qualitatively, images (Figure 5) of the oligomer (β's) in uranyl formate layers are composed of three or four regions of high-beam intensity[4] in which two to four maxima are distinguishable, delineated by lines of low beam intensity. The maximum dimensions of all monomer projections are identical, within the error of measurement, at 90 ± 5 Å, either in acetate or formate.

[4] Throughout the text, intensity variations are referred back to the intensity of the electron beam at the image plane. Regions in the image produced by high-beam intensity, and representing object regions relatively free of heavy metal, appear dark in the zero and even-numbered stages of contrast enhancement and light in the odd-numbered stages.

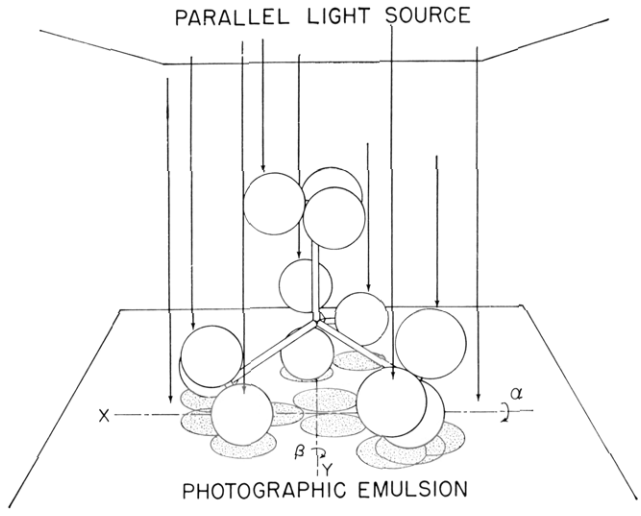

FIGURE 6: Schematic of light shadowgraph simulation of electron imaging. The model, in this case composed of four trimeric masses, each located at a vertex of a tetrahedron, is placed on the emulsion side of photographic paper attached to a surface which can be tilted relative to incident parallel light. The size and separation of the balls, which represent tightly folded protein cores not penetrable by heavy metal, were normalized to the dimensions observed in the particle projections.

The characteristic forms of projections, in decreasing order of abundance in the micrographs, are A (see Figure 5), the dominant form, a propeller shape with three broad blades and a central hub of high intensity, each composed of two or three distinguishable intensity maxima; B, a propeller shape with three broad blades of high intensity, each composed of three or four distinguishable maxima, arrayed around a region of low intensity; and C, a rectangular form with two bars of high intensity, one along one end and the other along one side, each composed of two or three distinguishable maxima, and a less well-defined region of high intensity occupying the opposite side and end. Projections like AB (Figure 5) appear to represent extensively disrupted particles, and although they occur infrequently, they demonstrate clearly the delineation of three clusters composed of three or four maxima.

Studies on particle dimensions (to be published elsewhere) demonstrated that the GDH β unit adhering to carbon substrate enlarges an average of 30 Å in dilute solutions of uranyl salts. Thus, as a first approximation in interpreting the micrographs, it was assumed that lines of low-beam intensity in the images of the particles represented heavy metal which had penetrated into the particle, causing it to swell, and that the dimensions of the penetrating species were very small relative to the particle dimensions. Light shadowgraphs of "wire-and-ball" models are then ready analogs for electron imaging (the oscilloscope display method of Kiselev and Klug, 1969, was not available). A variety of models, including the model proposed by Horne and Greville (1963) were tested. A schematic of the procedure, using the model giving best fit with the micrographs, is presented in Figure 6. Shadowgraphs of the model, consisting of four "trimeric" subunits with centers at the vertices of a tetrahedron, are presented in Figure 7. The length of the tetrahedral axes and the size of fold-ons were normalized to the dimensions on the micrograph. The different projections were obtained by varying the tilt of the supporting plane relative to the light rays or by varying the array of fold-ons supporting the model on the support surface (details in legend). Shadowgraph projections equivalent to A, B, and C

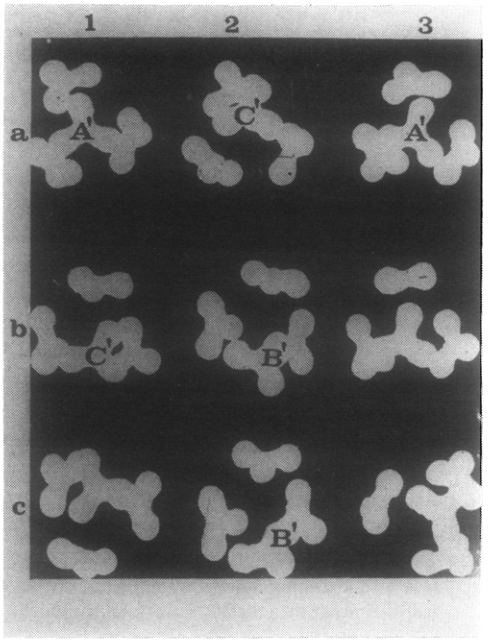

FIGURE 7: Light shadowgraphs of the "best-fit" wire-and-ball model described in Figure 6. Projections in column 1 were obtained when one tetrahedral axis was oriented perpendicular to the supporting plane, as shown in Figure 6, so that the model was supported by one fold-on from each of three subunits. Those in column 2 were obtained by rotating the configuration in Figure 6 about one tetrahedral axis so the support was two fold-ons from the subunit centered on the rotation axis and one fold-on from a second subunit. Those in column 3 were obtained by inverting the configuration in Figure 6 so that one subunit provided all three support surfaces. Rows b and c show projections obtained by tilting the support plane about the x and y axes in Figure 6; 1b, $\alpha = -30°$; 1c, $\alpha = 30°$; 2b, $\alpha = -30°$; 2c, $\alpha = -30°$, $\beta = 10°$; 3b, $\alpha = -30°$; 3c, $\beta = 20°$.

are labeled A′, B′, and C′, in Figure 7. The "goodness-of-fit" was found to be dependent on the rotation of the trimeric subunits about the tetrahedral vertices, with best fit obtained by orienting each fold-on on a line from the vertex of the tetrahedron to the vertex of the circumscribing regular icosahedron. In particular, projections obtained by rotating the subunit analogs, so each fold-on lies on a line between a vertex of the closely related cuboctahedron (or Dymaxion of Buckminster Fuller; see Marks, 1960) and a vertex of the tetrahedron, give poor fit. As described below, this distinction is not possible with a more realistic simulation procedure. Projections of the pyramidal model of Horne and Greville and ring models gave negligible fit with the micrographs.

The light shadowgraph procedure is an oversimplified analog of what may occur in the stain layer, *i.e.*, it ignores the effects on projections observed microscopically of asymmetrical penetration or disruption of the protein particle by heavy metal, as well as the effects of depth of immersion in the stain and the effective packing dimensions of the stain. As shown in Figure 5, the dimensions of the smallest identifiable metal-free regions is less than 20 Å for all three projection categories. Under these conditions, it cannot be assumed that the dimensions of the metal salt species in the stain layer are negligibly small relative to the substructural element, and either light shadowgraphs or oscilloscope display methods could be misleading; thus it is useful to interpret the micrographs in terms of the interplay of two kinds of effects: those arising from perturbation of a packing array in the negative stain layer by the protein particle, and those arising from disruption and penetration of the particle by stain.

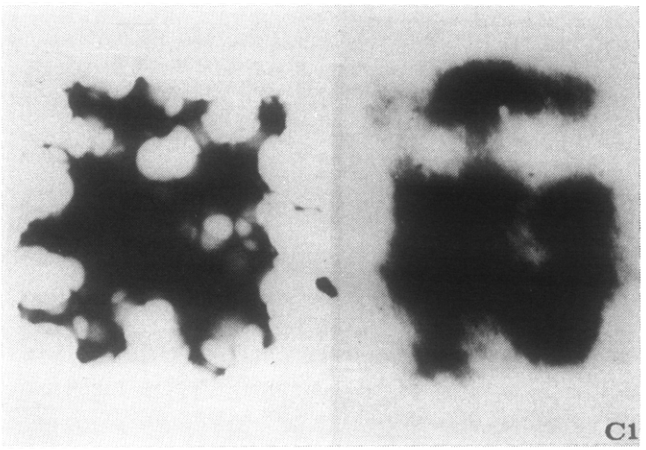

FIGURE 8: Comparison of X-ray shadowgraph and electron image projections of category C. Simulation employed a model comprised of twelve polystyrene spheres in an icosahedral array, submerged in marbles so that a layer one marble thick covered the particle, with no penetration of marbles or disruption of the model. Dimensions, normalized to a maximum projection dimension of 90 Å, are 37 Å, fold-on diameter; 97 Å, maximum dimension of the model; and 16 Å, marble diameter.

A straightforward extension of X-ray shadowgraph technique (for details, see under Methods) was employed to quantify these effects. By varying the size of the polystyrene spheres used in constructing the model and of the glass beads simulating the stain layer, effective packing dimensions of 5, 9, 10, and 16 Å in the stain layer were obtained. The intensity of X-irradiation and exposure were adjusted to give contrast levels of from 2 to 10% per bead, according to the numbers given by Haine (1961) for contrast levels from heavy metal atoms or their aggregates. A variety of models was tested.[5] Comparison of Figure 5 to the shadowgraphs confirmed that, as observed with light shadowgraphs, best fit is obtained with a model composed of four trimeric subunit analogs, with the fold-ons arrayed at the vertices of an icosahedron.

Figure 8 compares a rectangular form C from Figure 5 with the X-ray analog. The precision of fit is remarkable with this projection, obtained with the X-ray procedure from any totally submerged model made of twelve spheres in an icosahedral array, *i.e.*, there is no penetration of beads or disruption of the oligomer model. Figure 8 illustrates our conclusions from the X-ray shadowgraphs: (a) lines of low-beam intensity within particle projections do not necessarily reflect stain penetration into the particle, and as likely reflect the packing characteristics of the stain layer, as in this example; (b) by the same token it is obvious that maxima in regions of high beam intensity (*i.e.*, regions in the object containing little heavy metal) may not be directly interpretable as fold-on structures, nor a collection of maxima (*e.g.*, the bars on the end or one side of projection C–C′) as a subunit; (c) the lateral extent of the particle is obscured by the stain layer, giving projection dimensions smaller than those of the particle; (d) the dimensions

[5] The models tested included the pyramidal model of Horne and Greville; dodecahedra composed of four trimeric subunits, or six dimeric subunits with either a threefold or a fourfold axis; cuboctahedra composed of four trimeric or six dimeric subunits; irregular polyhedra composed of five or six trimeric subunits; a close-packed structure composed of five dimeric subunits; and a solid pyramidal structure composed of five dimeric subunits.

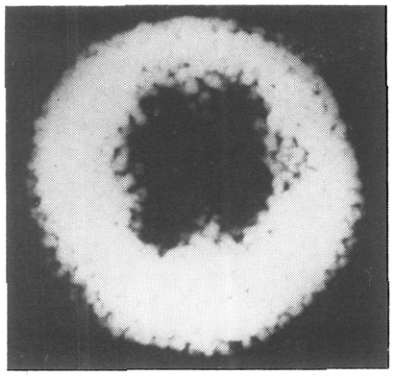

FIGURE 9: X-Ray shadowgraph with simulated 9-Å stain dimension. Model and simulation as in Figure 8, normalized marble dimension 9 Å.

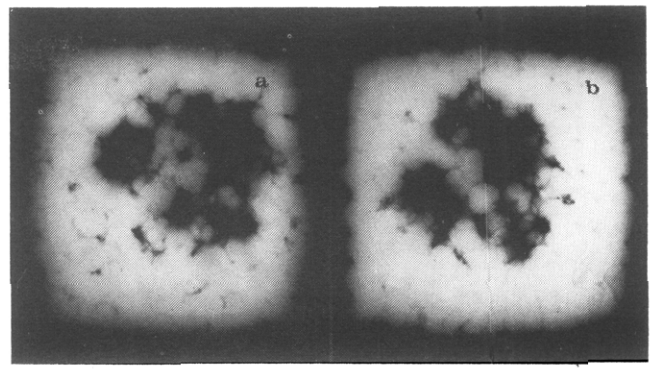

FIGURE 10: X-Ray shadowgraphs simulating propeller-shaped projections. Simulation performed as described for Figure 8, employing a tetrahedral model comprised of four subunits, each made of three polystyrene spheres (icosahedral array), penetrated by marbles through subunit–subunit contacts. Model aligned with one tetrahedral axis parallel to the incident radiation, as in Figure 6. In b the central void was solidly packed with marbles. a and b correspond to projections A and B, respectively, in Figures 4 and 5. Dimensions as described for Figure 8.

and shape of the projections vary appreciably with the depth of stain, and best fit with the micrographs is obtained with total submersion of the models; (e) the packing dimensions in the stain layer have a pronounced effect on the observed shadowgraph. As shown in Figure 9, for packing dimensions analogous to 9 Å in the stain layer, the shape of projection C′ appears more regular, and details of the surface are less well defined. The 16-Å (Figure 8) packing dimension gave shadowgraph detail more closely equivalent to the electron microscopic images than detail obtained with the 10-Å packing dimension. The X-ray shadows of submerged, unpenetrated, models made of twelve fold-ons in a cuboctahedral array also give rectangular projections with contrast distributions equivalent to those observed microscopically. Furthermore, both the icosahedral and cuboctahedral arrays can be distorted by compression in the plane of the stain layer analog (up to an axial ratio of 0.8) without destroying the equivalence of the shadowgraphs and electron micrographs.

Propeller-shaped shadowgraph projections were obtained when models were distorted, either by permitting the X-ray opaque beads to penetrate into the structure through broken intersubunit contacts, or by compressing the model along the apparent threefold axes. Of the models described above, only four closely related basic structures gave significant agreement with the micrographs. Figure 10, corresponding to particle A1 in Figure 5, is typical of the detailed agreement obtained with the icosahedral array composed of four trimeric subunits. Good correspondence between projections of the cuboctahedral array (the Dymaxion of Buckminster Fuller), composed of four trimeric subunits, and the micrographs was also observed. Projections obtained with icosahedral array composed of six dimeric subunits, with all subunit–subunit contacts penetrated by beads, gave poor fit with micrograph projections. However, as shown in Figure 11, if the six dimeric subunits are constrained into three tetrameric masses (γ,?) in either icosahedral or cuboctahedral arrays, fit with the micrographs is excellent.[6] In simulation with penetrated models the intensity distribution in the central region of the projections was determined by both the configuration of the uppermost surface of the submerged model, and by the penetration of beads into the central void space. Projections corresponding to category B in Figure 5 were obtained either if the fold-ons comprising the upper surface were spread apart by penetrating opaque beads, or if the central void were packed with beads. If the fold-ons on the upper surface were in close contact (for example, at intrasubunit fold-on contacts) and if the central void contained few opaque beads, projections of type A were obtained.

Projections in Positive Stain. Efforts were made to stain GDH positively with $TlHCO_3$, HgI_2 (both as ethanol solution and as a vapor), and uranyl salts. The Thallous stained particles were detectable at low magnifications, but the contrast at higher magnifications remained negligible after three stages of contrast enhancement. Adequate contrast was obtained with 1% HgI_2 in ethanol, but the particles were extensively disrupted. GDH stained with dilute (0.1 M) uranyl acetate was detectable at high magnification, but gave little structural information (Figure 13) after three stages of photographic contrast enhancement. As shown in Figure 12, excellent con-

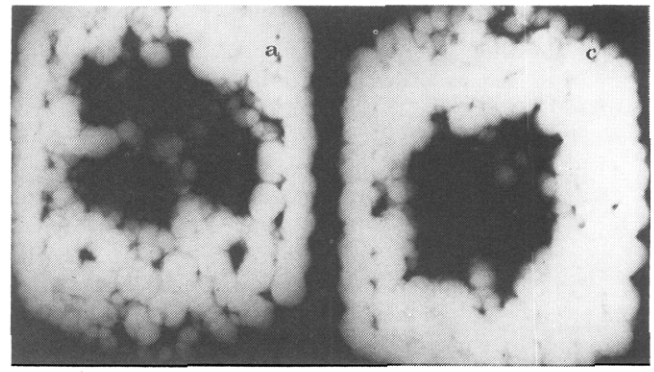

FIGURE 11: X-Ray shadowgraphs simulating micrograph projections. Simulation performed as described for Figure 8, employing a octahedral model comprised of six subunits, each made from two polystyrene spheres (icosahedral array), but with subunits constrained into three tetrameric masses by marble penetration through the n–n contacts shown in Figure 17. a and c correspond to projection categories A and C, respectively. The threefold symmetry axis was aligned parallel to the incident radiation in a and perpendicular to it in c. Dimensions as described for Figure 8.

[6] In order to obtain shadow projections equivalent to the micrographs using dimeric subunit models, it is necessary to postulate at least two types of intersubunit contacts, one more susceptible to disruption by stain than the other. This in effect divides the oligomer into three tetrameric masses, and the justification of the postulate is an immediate consequence of the symmetry considerations below.

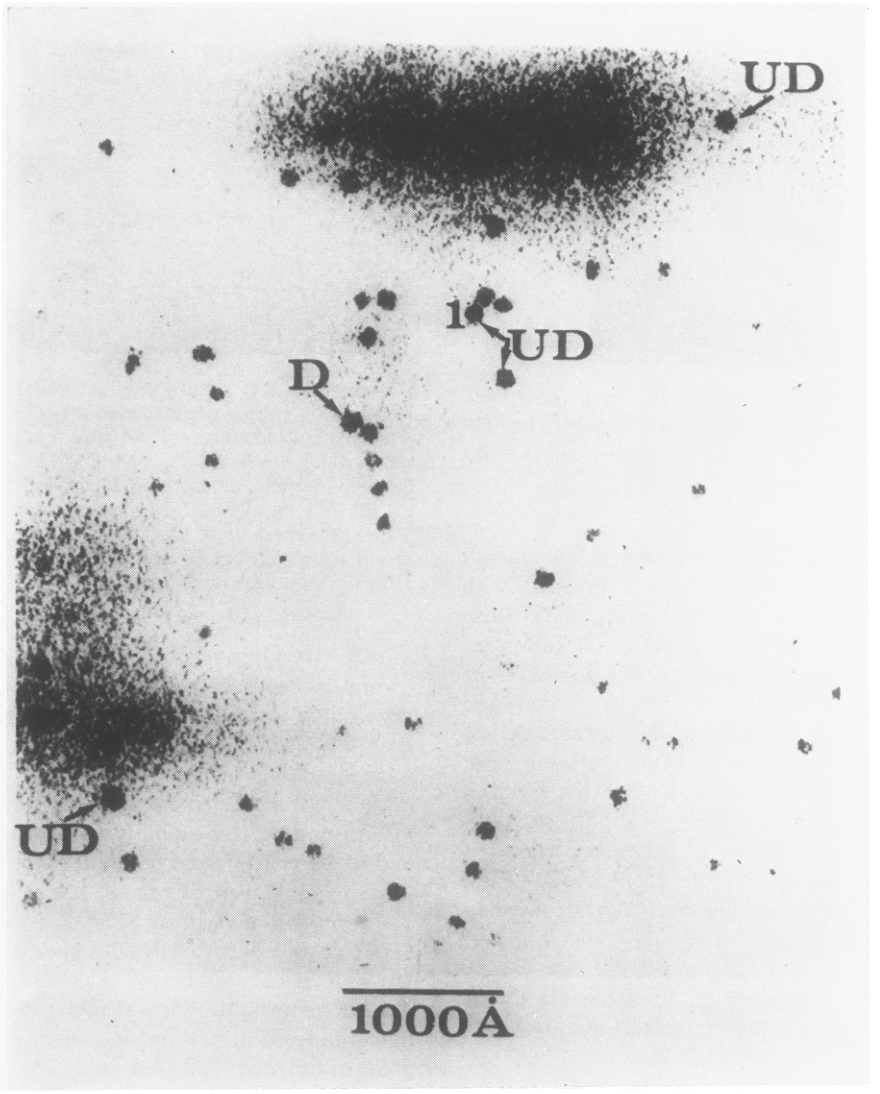

FIGURE 12: GDH positively stained with 1% uranyl acetate. Protein deposited from solution of 0.05 mg of GDH/ml of solution A, and stained for 2 min. After five stages of photographic contrast enhancement, magnification 180,000×. Disrupted and undisrupted β particles labeled D and UD, respectively.

trast was obtained by deposition of uranyl acetate from concentrated solution (1%), in areas of the substrate where thin layers of the salt had dried. Most projections of undisrupted particles (UD, Figure 12) appear hexagonal. As shown in Figure 13, this is predicted by the X-ray shadowgraph analog of positive staining with an icosahedral array of fold-ons. It is striking that a slightly disrupted particle (D, Figure 12) has projection detail equivalent to that obtained in negative stain, and that the distribution of heavy metal defines precisely the same projected distribution of mass suggested by negative stain (projections A, Figure 5), *i.e.*, a central mass surrounded by three separate masses, each divided into two or three components. Agreement in such detail supports the conclusion that the structural detail in projections in negative stain cannot be attributed to artifact. The dimensions of the positively stained, undissociated particles vary considerably over the grid (120–150 Å), in proportion to the thickness of the uranyl acetate layer deposited on the substrate.

Projections of Suboligomers Stained Positively. One of us (H. F. Fisher and L. L. McGregor, unpublished work) has studied the viscosity of GDH solutions as a function of SDS concentration during dissociation by this reagent. The initial effect of SDS at low concentration (3 mM) is a decrease in viscosity, accompanied by a decrease in weight-average molecular weight, as measured by light scatter. The decrease in viscosity suggests that dissociation by 3 mM SDS yields suboligomers preserving a compact tertiary structure (Jirgensons, 1961). Grids bearing GDH dissociated by SDS and deposited on carbon substrates were prepared as described under Methods, and stained by the nonspecific deposition of uranyl acetate, as described above.

The suboligomers were difficult to detect visually on the screen; thus, high resolution through-focal series were taken of thin uranyl acetate films selected randomly at low magnification. It is evident from the observed projections that most, if not all, tertiary structure is maintained under these conditions, and both partially dissociated β particles of GDH (D) and suboligomers (S) are identifiable in Figures 14 and 15. The projections of suboligomers, either lying free on the supporting film or bound together in the partially dissociated β particles, are predominantly trimeric in appearance. It is apparent that one or more fold-ons of the suboligomers could be ob-

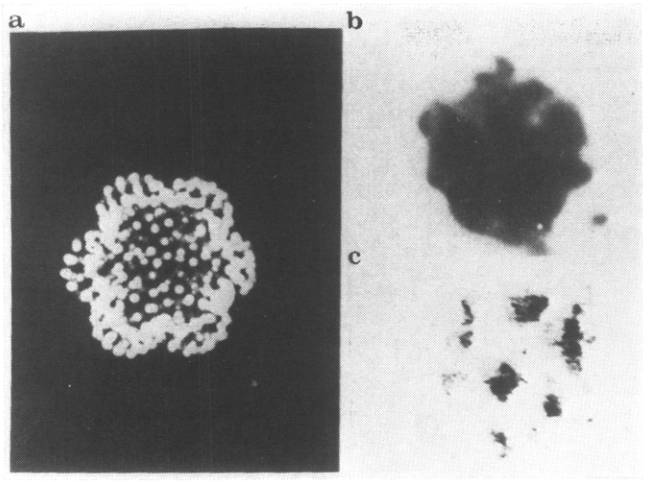

FIGURE 13: Comparison of projections in positive stain to X-ray shadowgraph simulation. (a) X-ray shadowgraph of a dodecahedral model comprised of twelve polystyrene spheres, with a single layer of glass beads closely packed onto all exposed surfaces; (b) projection UD1 in Figure 12; (c) projection of GDH positively stained with 0.01 M uranyl acetate (30 min), after three stages of photographic contrast enhancement

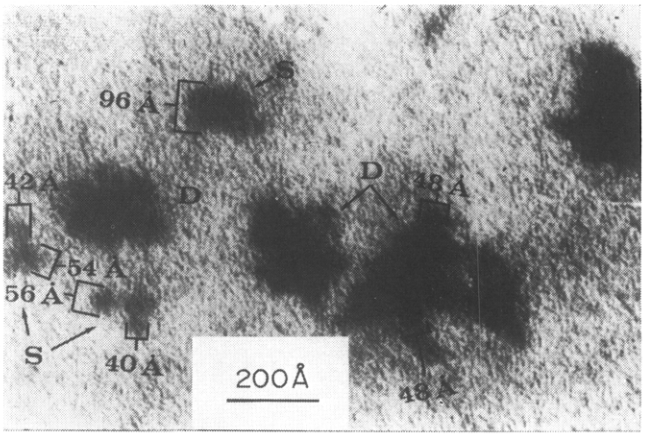

FIGURE 14: GDH treated with 3 mM SDS and positively stained. Protein was deposited and stained as in Figure 12. Labels are D for disrupted β units and S for the free-lying suboligomers. After three stages of photographic enhancement magnifications are 500,000× in Figure 14 and337,500× in Figure 15.

scured in the trimeric projections. The rectangular projections observed less frequently can be interpreted as an alternative projection of suboligomers composed of four fold-ons, or they can be interpreted as trimeric forms covered with a layer of uranyl salts sufficiently thick to obscure a trimeric substructure. The dimensions of a single fold-on within trimeric projections (45 ± 8 Å) agree well with a calculated 49 Å (for a 125-Å uranyl-stained particle composed of twelve spherical masses packed in a dodecahedron). The dimensions of the rectangular S particles are consistently about twice the average dimensions of one fold-on, supporting the alternative possibility that the S particle is, in fact, tetrameric. This is consistent with the projections in negative stain, where some particles (B–AB, Figure 5) appear to be divided into three clusters of three or four metal-free regions.

Alternative Proposals for GDH Quaternary Structure. The evidence presented above suggests that (a) GDH is a globular mass with maximum dimensions 90 ± 5 Å (either from negative stain or shadow dimensions), (b) that it is an oligomer composed of twelve morphological units (fold-ons) occupying nearly equivalent environments, and (c) that the twelve fold-ons are arrayed approximately at the vertices of either an icosahedron, or the closely related cuboctahedron. The data do not establish how the fold-ons are distributed in subunits, but do limit the alternatives. Of the many models tested here only four give X-ray shadows equivalent to the electron images. (1) A model (Figure 16a) composed of four subunits (each composed of three covalently bonded fold-ons) located at the vertices of a tetrahedron and oriented so each fold-on defines one vertex of an icosahedron. (2) A model (Figure 16b) identical with point 1, but with the trimeric subunits rotated so each fold-on defines one vertex of a cuboctahedron. (3) A model (Figure 16c) composed of six subunits (each made of two covalently bonded fold-ons) located at the vertices of an octahedron, and oriented so each fold-on defines one vertex of an icosahedron, and (4) A model (Figure 16d) identical with point 3, but with the dimeric subunits rotated so each fold-on defines one vertex of a cuboctahedron.

As mentioned previously, all of these models can be compressed along an apparent threefold axis through the center of the models, up to an axial ratio of 0.8, without destroying the equivalence of the shadow projections and projections in the electron images.

Both the icosahedral and cuboctahedral arrays are relatively open structures encompassing a central void space, which conforms to the predictions of Sund *et al.* (1969) derived from X-ray scattering. The radii of gyration of the models are also close to the low-angle X-ray data; for example, a 95-Å model composed of twelve 36-Å spheres in an icosahedral array has a radius of gyration of 30.2 Å about any axis passing through the center of the model, compared to the 30.3-Å average cross-sectional radius of gyration given by Sund *et al.* Furthermore, the dimensions of the compressed forms of the models giving adequate fit with the micrographs, with major and minor axes of 95 ± 5 and 75 ± 5 Å, respectively, are in the same range as those suggested by Sund on the basis of a cross-sectional anisotropy of 0.8. The extent of agreement between Sund's and our laboratory's results is, however, puzzling when the calculated mass density is considered. The minimum β-particle density consistent with the 95-Å maximum dimension and 280,000 molecular weight is 2950 g/l (Å mole) in both cases. Thus a maximum dimension of 95 Å represents a much more compact structure than the 2340 g/l (Å mole) predicted by Sund *et al.*

Model Symmetries. The possible symmetries of subunit

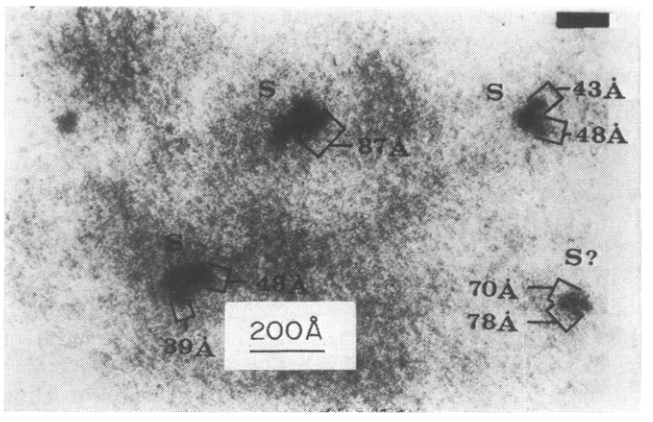

FIGURE 15: See caption to Figure 14.

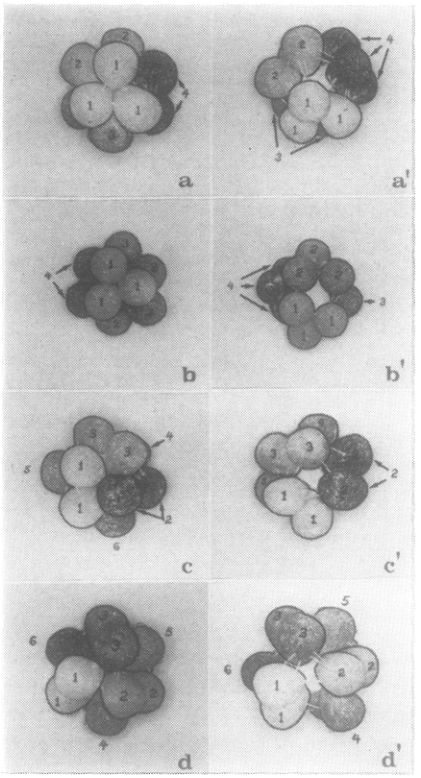

FIGURE 16: Alternative models for GDH quaternary structure. The model in frame c is typical of the models, made from spherical fold-on analogs, while the other frames show models comprised of fold-ons generalized in shape to fill more of the volume defined by the particle. The primed frames present the models disrupted at the subunit-subunit contacts. (a–a′) Comprised of four trimeric subunits, each centered on a vertex of a tetrahedron, and rotated so each fold-on defines a vertex of an icosahedron; (b–b′) comprised of four trimeric subunits, each centered on a vertex of a tetrahedron and rotated so each fold-on defines a vertex of a cuboctahedron; (c–c′) comprised of six dimeric subunits, each centered on a vertex of an octahedron, and rotated so each fold-on defines a vertex of an icosahedron; and (d–d′) comprised of six dimeric subunits, each centered on a vertex of an octahedron, and rotated so each fold-on defines a vertex of a cuboctahedron.

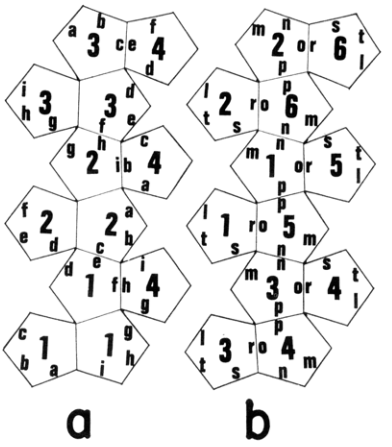

FIGURE 17: Representation of subunit contacts in symmetrical models. (a) The general case for trimeric subunits with fold-ons in an icosahedral array, each subunit having nine (a–i) contact surfaces, and (b) the general case for dimeric subunits with fold-ons in an icosahedral array, each subunit having eight (l–t) contact surfaces. The point group symmetries of the models, *D*2 for 2a and *D*3 for 2b, are evident if the figures are folded so each contact between fold-ons lies on an edge of a regular dodecahedron.

contacts in the proposed models were examined for a general case, *i.e.*, assuming identical asymmetric subunits and making no assumptions regarding equivalence of the fold-ons within subunits. For this general case trimeric subunit models have nine nonequivalent intersubunit contact surfaces, while dimeric models have eight. For each of the models described in this section there is only one orientation of subunit analogs which places each subunit (and consequently each fold-on) in equivalent environments. The required orientations for models in the icosahedral array are shown in Figure 17, and can best be visualized by copying the figure, cutting out the pattern, and taping it together to form the contact model.

The symmetrical tetrahedral model in this array has three orthogonal twofold axes, with point group symmetry *D*2. The conversion to a cuboctahedral array, accomplished by rotating each subunit about one axis of the base tetrahedron, changes the intersubunit contacts, but the symmetry remains the same, point group *D*2. Comparing the trimeric contact model to Figure 6, we see that the axes of the base tetrahedra, which appear to be threefold axes of rotation in terms of mass distribution, qualify only if all fold-ons are identical. However for interpretation of micrographs in terms of the parameters which determine the projections of an oligomer, *i.e.*, the distribution of (a) mass and (b) regions penetrable by stain, the tetrahedral axes must be regarded as very real threefold axes of rotation. For the tetrahedral models there does not appear to be a straightforward way to build an anisotropic form with equivalent subunit environments.

The symmetrical octahedral model in the icosahedral array is characterized by one threefold axis of rotation and three twofold axes in a plane perpendicular to it (point group *D*3). Again conversion into the cuboctahedral array is accomplished by rotating each of the six dimeric subunits about the axes from the center to the vertices of the octahedral base, which changes the intersubunit contacts, but maintains the *D*3 point group symmetry. For the octahedral models an anisotropic cross section is an immediate consequence of assuming a difference in the size of the two component fold-ons, and the resulting models maintain the same point group symmetry.

Examination of the dimeric contact surfaces (Figure 11) shows a structural rationale for subdividing the model into three tetrameric masses, which, as described above, is necessary for obtaining fit with the micrographs. With the designation in the figure, there are three intersubunit contacts comprised of a chain of three fold-on contacts, r–o, p–p (defining a twofold axis of rotation in the folded model), o–r. These contacts between subunits 3 and 4, 1 and 5, and 2 and 6, represent the only occurrences of intersubunit contacts through more than 2 contact surfaces. If it is assumed that the strength of forces holding the subunits together is proportional to the number of intersubunit contacts, then this chain provides the strongest intersubunit bonds, leading to tight tetrameric structures. The next strongest bonds, according to this argument, should involve intersubunit contact through two surfaces, which as shown in Figure 17 are the chain of m–s, and l–t contacts. The tetrameric masses are in contact through one additional surface involving only one fold-on of each tetramer, the n–n contact. Disruption by heavy metal at this probable weak link in the structure would lead to the observed projections in negative stain.

Structural Concepts and the Models. The above arguments are only as valid as the analog used in interpreting the micrographs, and it is obvious that the approach we have employed

is still oversimplified. For example, the X-ray analog method described here does not consider binding of heavy metal at specific residues on the exterior, and perhaps the interior, of the protein particle; and it does not attempt to account for the probably wide distribution of ion complex dimensions characteristic of heavy metal ions in equilibrium with polyion species, either in the stain layer, at the surface of the protein particles, or within the void spaces of the particles. However, our studies do present compelling evidence that in GDH the subunits (asymmetric units) are divided into discrete morphological units, or fold-ons.

Some ambiguity in interpreting the micrographs presented here in terms of specific models of GDH quaternary structure can be dispelled by considering the next level of GDH structure, the formation of linear aggregates. Sund *et al.* (1968) demonstrates that for GDH aggregates the mass per unit length and the average cross-sectional radius of gyration are independent of the degree of aggregation; and that the dimension corresponding to one β unit in the aggregate is about 100 Å. The same conclusions are reached in studies of the dimensions of platinum shadows of the aggregates (to be published elsewhere), from which a 92 ± 5 Å dimension is deduced for the β unit. Sund's results suggest that if the β unit has an anisotropic cross section, the contacts between neighboring particles must occur at the surface with the short dimension so that the contacts are separated by the long (90–100 Å) dimension. This is not observed with the projections of aggregates observed in Figure 1. Propeller-shaped and rectangular β projections (described in detail in the negative-stain section) can be differentiated within the projections of the aggregates, and it is apparent that these two classes of β projections are not distributed in any recurring pattern; nor does either class occur in a set orientation relative to a line connecting the centers of the particles. In particular, the rectangular projections frequently occur with the short dimension lying parallel to the line connecting the centers of the particles. Consequently, if the rectangular projections were side views of particles with anisotropic cross sections, the average particle center-to-particle center distance in the aggregate would necessarily be less than the long dimension of the particle. This clearly is inconsistent with both the X-ray-scattering data and the shadow dimension data on the aggregates. The alternative explanation, that the different projections reflect differing degrees of disruption by penetrating heavy metal of nearly spherical β units (maximum dimension about 95 Å), thus seems more likely.

Whitehead (1965) observed that the molecular weights of the dehydrogenases cluster around points which can be predicted by assuming these enzymes are composed of a basic building block of about 20,000 molecular weight, with the possible numbers of building blocks defined by the number of faces of regular polyhedra. The above assumption led to publication of a theory of dehydrogenase structure (which was received by workers in this area with some skepticism), specifying that the subunits of the oligomeric species should be composed of one or more discrete masses with molecular weights in the range of 20,000. The electron microscopic evidence presented here is consistent with Whitehead's prediction of twelve fold-ons per functional oligomer (β) of GDH, and the fold-on dimensions correspond to molecular weights in the 20,000 range. Again, as predicted by Whitehead, lactic dehydrogenase has been shown by X-ray diffraction (Adams *et al.*, 1969) to be composed of eight protein masses, with each of the four subunits composed of two masses connected by a neck of protein. The fold-ons in lactic dehydrogenase are not the same size, one corresponding to more than 20,000 molecular weight, the other to less.

The occurrence of fold-on structure is not limited to dehydrogenases, as shown in studies of serum albumin (Bloomfield, 1966; Luzzati *et al.*, 1961; Foster, 1960; Harrington *et al.*, 1956). R. E. Gates and H. F. Fisher (personal communication) recently provided an attractive alternative to Whitehead's theoretical basis for a requirement for subdividing large protein masses, and the limiting dimensions they predict fall in the range observed in fold-on type structures. Their treatment is based on the observation that the distribution of polar and nonpolar (according to two different assignment schemes) amino acids in the protein sequences of a wide variety of proteins, is not significantly different than a random distribution. They show that if amino acids which are buried occupy randomly assigned positions in the sequence, it is very probable that the tertiary structure adopted will have at least one dimension less than 40 Å (from water to water). Roughly spherical structures with dimensions in the 30-Å range correspond to molecular weights less than 20,000; and the theory is qualitatively substantiated by the large number of proteins in this molecular weight range, and the existence of fold-ons of the same molecular weight range, or of clefts in the tertiary structure, in larger proteins, giving about 30 Å from water to water as predicted. Their results also suggest that one optimum arrangement for burying the maximum number of nonpolar amino acids in the large oligomeric proteins is an array of protein subunits which encloses a central void space, *i.e.*, as in the quaternary structures demonstrated for lactic dehydrogenase and postulated here for GDH.

The relative infrequency of projections with a strong central mimima (which would indicate a ring-type structure) and the predominance of projections of category A (Figure 6) in uranyl formate negative stain is clearly not consistent with the ring model proposed by Fisher (1969) and recently by Josephs (1970). However, the 3.2 point group symmetry suggested by Josephs is consistent with our data, and the primary difference between model 3 presented in Figure 16 and the model proposed by Josephs is the fold-on nature of the structure postulated in this paper. Although our data are consistent with division of the quaternary structure into either four trimeric subunits or six dimeric subunits constrained into three tetrameric masses, the balance of the evidence, and especially the molecular weight data, favors the model composed of six dimeric subunits. The data provide conclusive evidence for a fold-on structure in GDH, and we are studying a variety of dehydrogenases to determine if this is a basic structural phenomenon in these enzymes.

Acknowledgment

We thank Dr. J. E. Mellema and Dr. R. E. Gates for stimulating comments on the work.

References

Adams, M. J., Haas, D. J., Jeffrey, B. A., McPherson, A. Jr., Mermall, H. L., Rossman, M. G., Schevitz, R. W., and Wonacott, A. J. (1969), *J. Mol. Biol. 41*, 159.

Apella, E., and Tomkins, G. M. (1966), *J. Mol. Biol. 18*, 77.

Bloomfield, V. (1966), *Biochemistry 5*, 684.

Eisenberg, H., and Tomkins, G. M. (1968), *J. Mol. Biol. 31*, 37.

Fernandez-Moran, H., van Bruggen, E. F. J., and Ohtsuki, M. (1966), *J. Mol. Biol. 16*, 191.

Fisher, H. F. (1969), *in* The Mechanism of Action of Dehy-

drogenases, Schwert, G. W., and Winer, A. D., Ed., Louisville, Ky., The Univ. Press of Kentucky, p 179.
Fisher, H. F., and Cross, D. G. (1962), *Nature (London) 196*, 895.
Fisher, H. F., McGregor, L. L., and Power, U. (1962), *Biochem. Biophys. Res. Commun. 8*, 402.
Fiskin, A. M., and Beer, M. (1968), *Science 159*, 1111.
Foster, J. F. (1960), *in* The Plasma Proteins, Vol. 1, Putnam, F., Ed., New York, N. Y., Academic Press, p 179.
Frieden, C. J. (1962), *J. Biol. Chem. 237*, 2396.
Frieden, C. (1964), *Brookhaven Symp. Biol. 17*, 98.
Haber, J. E., and Koshland, D. E. (1967), *Proc. Nat. Acad. Sci. U. S. 58*, 2087.
Haine, M. E. (1961), The Electron Microscope; The Present State of the Art, Chapter IV, New York, N. Y., Interscience.
Harrington, W., Johnson, P., and Ottewill, R. (1956), *Biochem. J. 62*, 569.
Haydon, G. B. (1969), *J. Micros. 89*, 251.
Heidenreich, R. D. (1964), Fundamentals of Transmission Electron Microscopy, New York, N. Y., Interscience, p 139.
Highton, P. J., and Beer, M. (1968), *J. Roy. Micros. Soc. 88*, 23.
Horne, R. W., and Greville, G. D. (1963), *J. Mol. Biol. 6*, 506.
Jirgensons, B. (1961), *J. Amer. Chem. Soc. 83*, 3161.
Josephs, R. (1970), Pyridine Nucleotide-Dependent Dehydrogenases, Berlin, Springer-Verlag, p 301.
Kirtley, M. E., and Koshland, E. E. (1967), *J. Biol. Chem. 242*, 4192.
Kiselev, N. A., and Klug, A. (1969), *J. Mol. Biol. 40*, 155.
Klotz, I. M., Langerman, N. R., and Darnall, D. W. (1970), *Annu. Rev. Biochem. 39*, 25.
Koshland, D. E., Nemethy, G., and Filmer, D. (1966), *Biochemistry 5*, 365.
Luzzati, V., Witz, J., and Nicolaieff, A. (1961), *J. Mol. Biol. 3*, 379.
Marks, R. W. (1960), The Dymaxion World of Buckminster Fuller, New York, N. Y., Reinhold, p 41.
Mellema, J. E., van Bruggen, E. F. J., and Gruber, M. (1967), *Biochim. Biophys. Acta 140*, 182.
Monod, J., Wyman, J., and Changeaux, J.-P. (1964), *J. Mol. Biol. 10*, 565.
Olsen, J. A., and Anfinsen, C. B. (1952), *J. Biol. Chem. 197*, 67.
Smith, E., Landon, M., Piszkiewicz, D., Bratton, W. J., Langley, T. J., and Melamed, M. D. (1970), *Proc. Nat. Acad. Sci. U. S. 67*, 724.
Sund, H., and Burchard, W. (1968), *Eur. J. Biochem. 6*, 202.
Sund, H., Pilz, I., and Herbst, M. (1969), *Eur. J. Biochem. 7*, 517.
Valentine, R. C., Shapiro, B. M., and Stadtman, E. R. (1968), *Biochemistry 7*, 2143.
Whitehead, E. P. (1965), *J. Theor. Biol. 8*, 276.
Wolff, J. (1962), *J. Biol. Chem. 237*, 230.

Nature of the Binding Site of Pyridoxal 5′-Phosphate to Bovine Serum Albumin*

John A. Anderson,† Hsai-fei Wang Chang,‡ and Carter J. Grandjean§

ABSTRACT: In the reaction between equimolar amounts of pyridoxal 5′-phosphate (PLP) and bovine serum albumin only one pyridoxyl peptide was found following reduction at pH 4.2–4.4 and subsequent digestion with trypsin. The amino acid sequence of the purified peptide was Ser-Leu-Phe-Glu-Lys-Pro-ε-(pyridoxyl)Lys-Lys. The presence of three lysine residues at the PLP binding site is consistent with the substituted aldimine structure as the species responsible for the 336-nm absorption peak of the PLP–albumin complex. The predominate species which absorbs at 330 nm in PLP–albumin–urea solutions is a PLP–urea product. The absorbance peak at 330–336 nm is small and there is a large 413-nm peak immediately after addition of urea to the PLP–albumin mixture. It is concluded that the PLP–albumin product with absorbance maximum at 336 nm is unstable in urea. The fluorescence of the 336-nm peak of PLP–albumin is quenched. Reaction of the tryptophans of albumin with *N*-bromosuccinimide did not affect the affinity, absorbance spectrum, or quenching of fluorescence of the binding site. Nitration of exposed tyrosines with tetranitromethane (10.7 tyrosines/mole of albumin) caused reduced binding of PLP to albumin. Quenching of fluorescence may be due to interaction with tyrosine residues.

Pyridoxal 5′-phosphate binds to the ε-amino group of lysine in proteins (*e.g.*, Kent *et al.*, 1958). There are several types of bound forms. One of these is the protonated Schiff base, which has an absorption maximum in the 410- to 430-nm region of the spectrum. In aspartate aminotransferase (Hughes *et al.*, 1962; Polianovsky and Keil, 1963; Morino and Watanabe, 1969) the Schiff base may not be protonated and the absorption maximum is shifted to the region of 360 nm. Finally, PLP[1] is bound in a form which absorbs maximally in the 330-nm region. This last species occurs in the neutral pH region, is unaffected by carbonyl reagents and is

* From the Department of Chemistry, Texas Tech University, Lubbock, Texas 79409. *Received December 28, 1970.* This work was supported by NSF Grant No. GB-6434 and by Robert A. Welch Foundation Grant No. D-117. Part of this work was done in partial fulfillment of the M. S. degree of H.-F. W. C. and of the Ph.D. degree of C. J. G.

† Present address: Massachusetts General Hospital, Boston, Mass.

‡ Present address: The Eppley Institute for Research in Cancer, Omaha, Neb.

§ Author to whom correspondence should be addressed.

[1] Abbreviations used are: PLP, pyridoxal 5′-phosphate; PTH, phenylthiohydantoin; TMN, tetranitromethane.